ACS APPLIED MATERIALS & INTERFACES

Research Article

www.acsami.org

Improving the Stability of Bulk Heterojunction Solar Cells by Incorporating pH-Neutral PEDOT:PSS as the Hole Transport Layer

Yanhong Meng, Zhanhao Hu, Na Ai, Zhixiong Jiang, Jian Wang,* Junbiao Peng, and Yong Cao

Institute of Polymer Optoelectronic Materials and Devices, State Key Laboratory of Luminescent Materials and Devices, South China University of Technology, Guangzhou 510640, P. R. China

Supporting Information

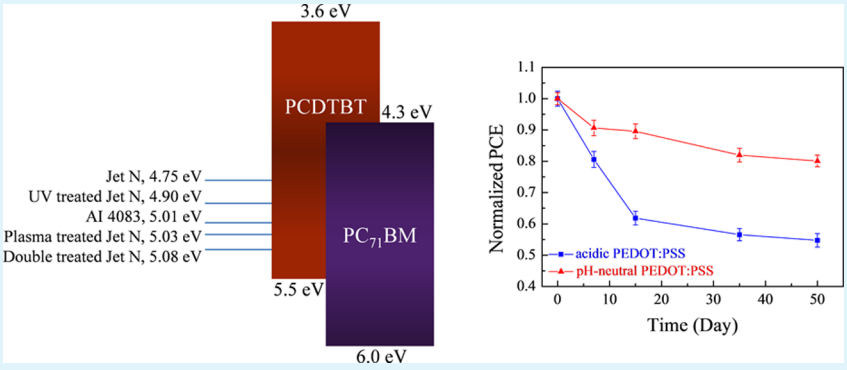

ABSTRACT: In the application of traditional bulk heterojunction polymer solar cells, to prevent the etching of ITO by the acidic poly(3,4-ethylenedioxythiophene):poly(styrenesulfonate) (PEDOT:PSS) and thereby improve the device stability, pH-neutral PEDOT:PSS is introduced as the hole transport layer (HTL). After treating the neutral PEDOT:PSS with UV-ozone and with an oxygen plasma, the average power conversion efficiency (PCE) of the device increases from 3.44% to 6.60%. Such surface treatments reduce the energy level offset between the HTL and the active layer, which increases the open circuit voltage and enhances hole transportation, leading to the PCE improvement. Moreover, the devices with the neutral PEDOT:PSS HTL are more stable in air than those with the acidic PEDOT:PSS HTL. The PCE of the devices with the acidic PEDOT:PSS HTL decreases by 20% after 7 days and 45% after 50 days under ambient conditions, whereas the PCE of the devices with the pH-neutral PEDOT:PSS HTL decreases by only 9 and 20% after 7 and 50 days, respectively. X-ray photoelectron spectroscopy shows that the acidic PEDOT:PSS etches the indium from the indium−tin−oxide (ITO) electrode, which is responsible for the degradation of the device. In comparison, the diffusion of the indium is much slower in the devices with the pH-neutral PEDOT:PSS HTL.

KEYWORDS: *polymer solar cell, PEDOT:PSS, hole transport layer, surface treatment, indium diffusion, stability*

INTRODUCTION

The bulk heterojunction (BHJ) polymer solar cell (PSC) has attracted much attention as a renewable energy source in both academic institutions and industry because of its easy fabrication, low cost, light weight, and capacity for fabrication on flexible substrates.[1−3] Considerable effort has been made to obtain a high power conversion efficiency (PCE),[4−10] which has exceeded 8% in a single-junction device.[11−14]

Traditional BHJ polymer solar cells consist of a transparent indium−tin−oxide (ITO) anode, a hole transport layer (HTL), a photoactive layer, and a top cathode. Poly(3,4-ethylenedioxythiophene):poly(styrenesulfonate) (PEDOT:PSS) is commonly used as the HTL in organic photovoltaic (OPV) devices. Additionally, various conducting polymers[15] and metal oxides,[16−19] such as NiO, MoO_3, V_2O_5, and WO_3, have been introduced as HTLs in OPVs. Recently, metal oxides have been deposited onto an ITO substrate using a solution process, which makes them potential candidates for the HTL in solution-processed polymer solar cells.[20−22] Nevertheless, PEDOT:PSS is still widely used as a robust solution-processed HTL to achieve a high PCE. Because of its high stability and water solubility, which allow facile preparation of the HTL through a conventional solution process, PEDOT:PSS is a better HTL material than other conducting polymers. However, the widely adopted PEDOT:PSS (AI 4083) has a pH value between 1 and 3 at 20 °C, which makes the interface between the ITO and the PEDOT:PSS unstable.[23] The acidic PEDOT:PSS etches the ITO, and the diffusion of the indium into the photoactive layer induces a fast degradation of the active layer.[24,25] Different approaches have been attempted to reduce the corrosion of the ITO by the acidic PEDOT:PSS. Inserting a self-assembled monolayer between

Received: January 16, 2014
Accepted: March 10, 2014
Published: March 10, 2014

 © 2014 American Chemical Society

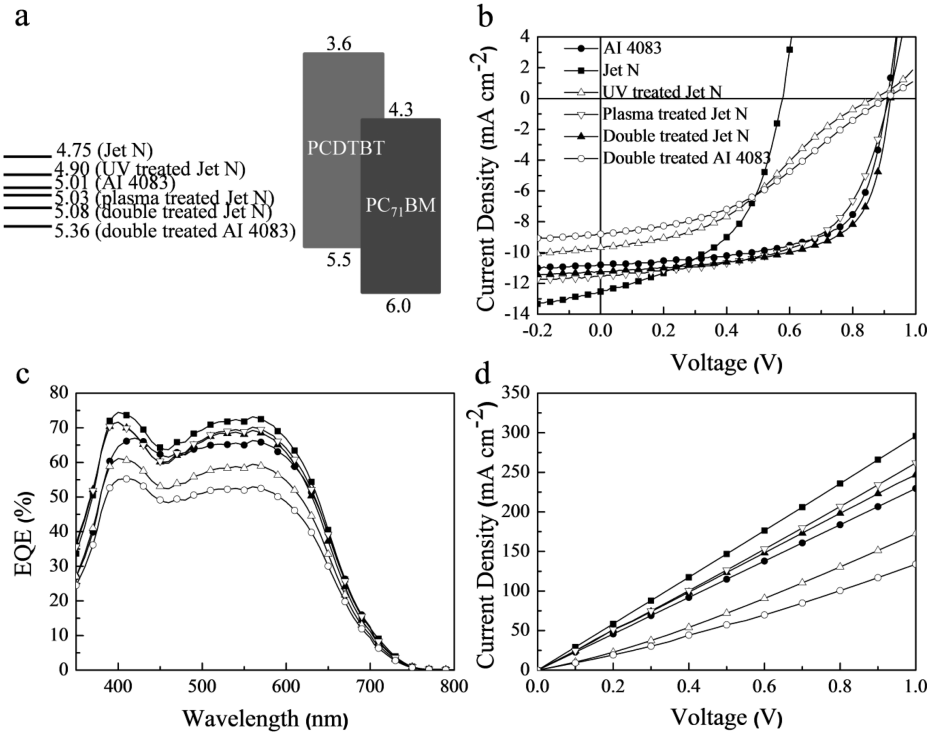

Figure 1. (a) Schematic illustrations of the energy levels of the devices. The units is eV. (b) *J*−*V* characteristics of the best-performance devices with different HTLs under 100 mW cm^{-2} air mass 1.5 global (AM 1.5G) illumination. (c) External quantum efficiency spectra of the devices with different HTLs. (d) *J*−*V* curves for different PEDOT:PSS layers in the device structure of ITO/PEDOT:PSS/Al.

the ITO anode and the HTL stopped the indium from penetrating into the HTL.[26] Kim et al. achieved a 25% improvement in lifetime by adding 0.2 M NaOH to the PEDOT:PSS solution to adjust the pH value.[27] The pH-neutral PEDOT:PSS has been successfully employed as a hole injection layer in the application of organic light emitting diodes.[28] However, a study on using pH-neutral PEDOT:PSS in OPVs has not been reported.

We replace the acidic PEDOT:PSS (AI 4083) HTL with a pH-neutral PEDOT:PSS (Jet N) in a BHJ device with a photoactive layer of poly[N-9″-hepta-decanyl-2,7-carbazole-*alt*-5,5-(4′,7′-di-2-thienyl-2′,1′,3′-benzothiadiazole)] (PCDTBT) that is doped with [6,6]-phenyl C_{71} butyric acid methyl ester ($PC_{71}BM$). Because of the limitations of our evaporation system, and to achieve a good device performance, we treated the active layer with methanol before the cathode deposition.[29−32] Without any surface treatment, the device with the pH-neutral PEDOT:PSS HTL has a PCE of only 3.44%, which is much less than that of the device with the acidic PEDOT:PSS HTL (6.28%). After treating the surface of the pH-neutral PEDOT:PSS with both UV-ozone and an oxygen plasma, the PCE increases to 6.60%. The improvement is attributed to the reduction of the energy level offset between the HTL and the active layer. The pH-neutral PEDOT:PSS stops the etching of the indium species in the ITO, which effectively protects both the ITO anode and the active layer. After 7 days of storage under ambient conditions, the PCE of the device with the acidic PEDOT:PSS decreases by 20%, whereas the PCE of the device with the pH-neutral PEDOT:PSS decreases by only 9%. After 50 days, the PCE of the device with the pH-neutral PEDOT:PSS decreases by 20%, whereas the PCE of the device with the acidic PEDOT:PSS decreases by 45%. The improvement in the lifetime caused by using the pH-neutral PEDOT:PSS is more than double.

RESULTS

In our experiment, 6 sets of 10 devices each were fabricated with an identical device structure of ITO/PEDOT:PSS/PCDTBT:$PC_{71}BM$/Al using the same fabrication process except for the surface treatments on the PEDOT:PSS films. The reference device (Device A) with the acidic PEDOT:PSS (AI 4083) as its HTL has an average PCE of 6.28% and a V_{OC} of 0.90 V. Replacing the acidic PEDOT:PSS with the pH-neutral version (Jet N) severely impacts the device performance. Device B with the Jet N HTL has an average PCE of 3.44% with a V_{OC} of 0.59 V. The fill factor (FF) is 49.1% compared with the FF of 62.9% of Device A. To improve the device performance, different surface treatments were applied to the Jet N films before depositing the active layer.

With five minutes of UV-ozone treatment (Device C), the device performance further drops. Though the V_{OC} recovers to 0.86 V, the average PCE drops to 3.06% with a FF of 36.6%. In contrast, treating the Jet N HTL with five minutes of oxygen plasma treatment (Device D) significantly enhances the device performance. The average PCE increases to 6.11%, and the FF increases to 58.9%. Applying both surface treatments, five minutes of UV-ozone followed by five minutes of oxygen plasma, provides the best result. Device E has an average PCE of 6.60%, a V_{OC} of 0.92 V, and a FF of 63.1%. This performance is even better than that of the reference, Device A. To examine the effects of the surface treatments on the acidic PEDOT:PSS HTL, Device F went through the same surface treatments as Device E. However, the double-treated AI 4083 deteriorates the device performance; Device F's average PCE is only 2.94%, and its FF is 37.0%.

dx.doi.org/10.1021/am500336s | ACS Appl. Mater. Interfaces 2014, 6, 5122−5129

Table 1. Performance of the OPV Devices with Different HTLs (measured under 100 mW cm^{-2} AM 1.5 G illumination)

device	HTL	J_{sc} (mA cm^{-2})	V_{oc} (V)	FF (%)	PCE (%)
A	AI 4083	11.0 ± 0.41	0.90 ± 0.01	62.9 ± 1.07	6.28 ± 0.05
B	Jet N	11.9 ± 0.39	0.59 ± 0.01	49.1 ± 1.50	3.44 ± 0.15
C	UV-ozone-treated Jet N	9.71 ± 0.07	0.86 ± 0.01	36.6 ± 1.03	3.06 ± 0.06
D	plasma-treated Jet N	11.5 ± 0.24	0.91 ± 0.01	58.9 ± 1.34	6.11 ± 0.05
E	double-treated Jet N	11.4 ± 0.28	0.92 ± 0.01	63.1 ± 1.69	6.60 ± 0.06
F	double-treated AI 4083	8.80 ± 0.07	0.89 ± 0.01	37.0 ± 1.93	2.94 ± 0.16

Figure 1a illustrates the energy diagrams of the devices. The current density−voltage (J−V) characteristics of the devices are presented in Figure 1b with the device performances summarized in Table 1. Figure 1c shows the external quantum efficiency (EQE) spectra of the devices. An increase in the EQE at wavelengths between 350 and 700 nm is observed in Device B, Device D, and Device E compared with Device A. The EQE enhancement contributes to an increase in the short circuit current density J_{SC} from 11.0 mA cm^{-2} in Device A to 11.9, 11.5, and 11.4 mA cm^{-2} in Devices B, D, and E, respectively.

DISCUSSION

Without a surface treatment, Jet N does not succeed as a good HTL in PSCs. The poor device performance can be attributed to the large energy level offset between the HTL and the active layer. As shown in Figure 1a, the energy barrier between the Jet N and the PCDTBT:$PC_{71}BM$ is substantially larger than that between the AI 4083 and the PCDTBT:$PC_{71}BM$. It is well known that the UV-ozone and oxygen plasma treatments can effectively enhance the work function.[33,34] To modify the interface between the Jet N layer and the active layer, we applied UV-ozone and oxygen plasma treatments to the Jet N layer. Scanning Kelvin probe measurements verify that after the UV-ozone treatment, the work function of the Jet N increases to 4.90 from 4.75 eV. After the oxygen plasma treatment, the work function increases to 5.03 eV, and after both treatments, the work function reaches 5.08 eV. The high work function of the HTL increases the built-in potential, which induces a larger internal electric field across the BHJ layer.[35,36] The enhanced internal field facilitates the separation of the photo-excited excitons and the extraction of both types of carrier and suppresses the charge recombination,[37,38] which leads to the improvement in the device performance.

In BHJ OPVs, the upper limit of the V_{OC} depends on the difference between the highest occupied molecular level of the donor and the lowest unoccupied molecular level of the acceptor when ohmic contacts are formed between the electrodes and the organic functional layers.[39] When a Schottky contact is formed, the V_{OC} is determined by the difference between the work functions of the electrodes.[40,41] Without any surface treatment, the V_{OC} of Device B is only 0.59 V in accord with the low work function of the Jet N. After surface treatments, the V_{OC} increases to 0.86 V, 0.91 V, and 0.92 V in the UV-ozone-treated device, the oxygen-plasma-treated device, and the double-treated device, respectively (Table 1). The improvements in the V_{OC} are consistent with the improvements in the work functions of the Jet N with the different surface treatments.

Another factor that enhances the performance is interface improvement. A large surface energy of the HTL could align the acceptor at the bottom of the active layer close to the HTL, which is not a preferable phase separation in carrier extraction. The desirable vertical phase separation has the acceptor close to the cathode to facilitate electron extraction and the donor close to the anode to facilitate hole extraction.[42] Therefore, it is necessary to reduce the surface energy of the HTL. The wettability of the HTLs was studied using contact angle experiments. The water contact angles on the AI 4083 and Jet N layers are 52 and 29°, respectively. After the surface treatments, the water completely wets the Jet N surface, which indicates that the surface energy of the double-treated Jet N is larger than that of the AI 4083. The large surface energy of the Jet N should degrade the device performance because of the non-ideal vertical phase separation. However, the double-treated Jet N device exhibits the best device performance. Therefore, we conclude that the enhancement of the device performance is not due to the change in the surface energy of the HTL.

In the case of the AI 4083 device, although the double-treatment increases the work function of the AI 4083 to 5.36 eV in Device F from 5.01 eV in Device A, Device F exhibits the worst device performance among all the devices. In addition, although the UV-ozone treatment improves the Jet N work function in Device C, Device C has an inferior performance in terms of PCE and FF compared with Device B. We believe that the poor device performance results from the large R_s. From Figure 1b, the R_s of Device C is 48.2 Ω cm^2 and the R_s of Device F is 76.3 Ω cm^2, which are one order of magnitude higher than the R_s values of the other devices (e.g., 4.90 Ω cm^2 in Device A and 3.75 Ω cm^2 in Device B). To investigate the root cause of the large R_s values, the electrical conductance of the PEDOT:PSS films with and without the surface treatments were measured with the device structure of ITO/PEDOT:PSS/Al. The J−V characteristics are shown in Figure 1d. The electrical conductance of the PEDOT:PSS film is highest in the Jet N followed by the plasma-treated Jet N, the double-treated Jet N, the AI 4083, the UV-ozone-treated Jet N, and the double-treated AI 4083 (the lowest), which is the same trend seen in the short circuit current density J_{SC} of the devices (Table 1). Although the UV-ozone treatment increases the work function of the Jet N and the double surface treatment increases the work function of the AI 4083, the sharp decreases in the electrical conductance lead to the significant increases in R_s that substantially degrade the device performances.

The resistance of the HTL depends on its thickness. On one hand, increasing the thickness of the double-treated Jet N film increases its resistance and thereby R_s, which degrades the device performance. On the other hand, because PEDOT:PSS is a hole-transporting material with poor electron-blocking properties, a very thin layer of AI 4083 cannot suppress the dark current effectively (Figure S1 in the Supporting Information),[43] which also degrades the device performance. Therefore, the optimized thickness of the HTL needs to achieve a balance between R_s and dark current (Table S1 in the Supporting Information). As a result, the optimal thicknesses of

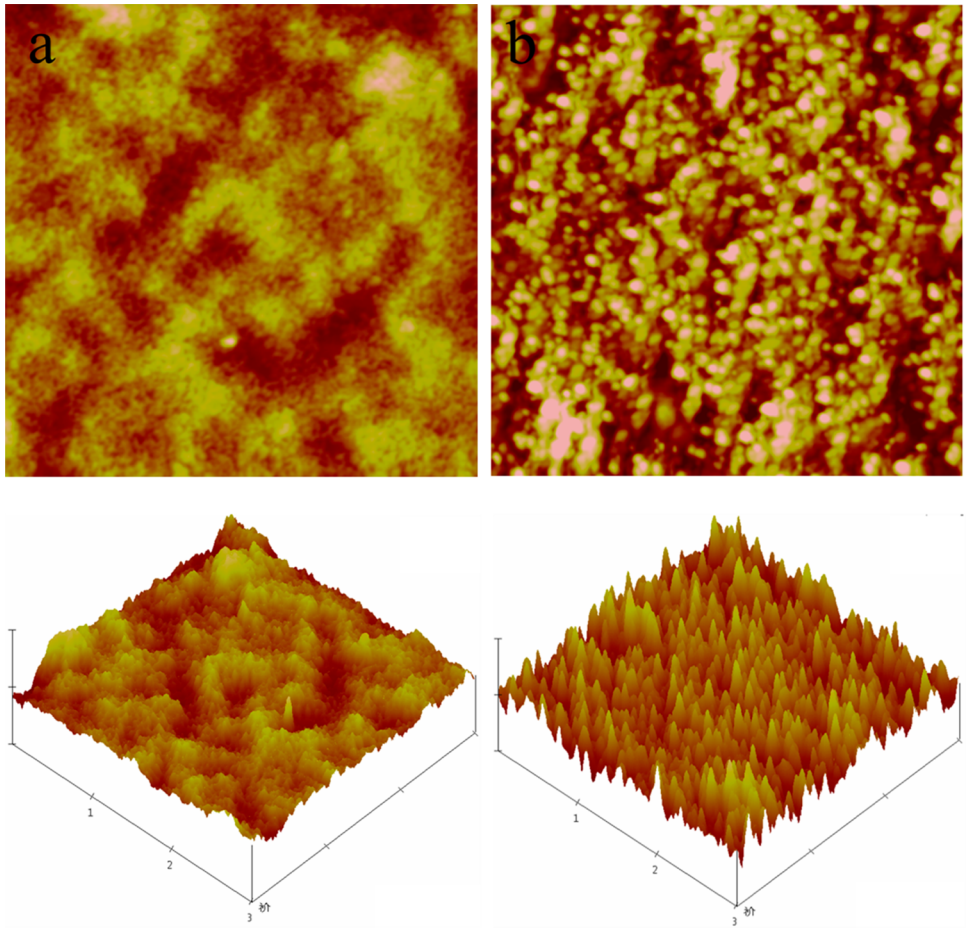

Figure 2. AFM topographic images of (a) double-surface-treated Jet N, and (b) oxygen-plasma-treated Jet N. The scan area is 3 μm × 3 μm.

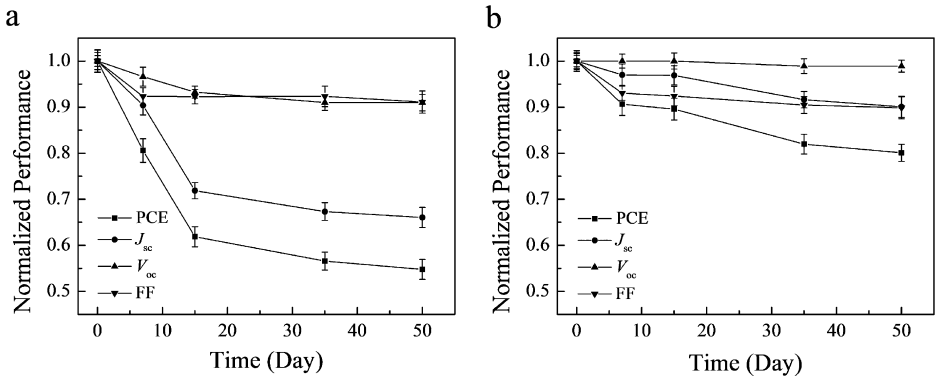

Figure 3. Dependence of the normalized device characteristics on storage time. (a) AI 4083 HTL device, and (b) double-surface-treated Jet N HTL device.

the AI 4083 and of the double-treated Jet N are 40 and 10 nm, respectively.

The oxygen-plasma-treated Jet N (Device D) has a work function and conductivity similar to those of the double-surface-treated Jet N (Device E), and both devices have the same V_{OC} and J_{SC}. However, the PCE of Device D is slightly lower than the PCE of Device E. We carefully examined the surface morphologies of the double-treated and plasma-treated Jet N films using atomic force microscopy (AFM) and found that the oxygen-plasma-treated Jet N film has a rougher surface. As shown in Figure 2, the surface roughness of the double-treated film is 2.01 nm, whereas the surface roughness of the oxygen-plasma-treated film is 3.73 nm. A rough interface between the HTL and the active layer is likely to induce a leakage current and to form trap states, thereby lowering the fill factor and the power conversion efficiency.[19,30]

The AFM topographic images of the PCDTBT:PC_{71}BM active layer on the AI 4083, the Jet N and the double-surface-treated Jet N show similar surface morphologies (see Figure S2 in the Supporting Information). The surface roughnesses are 0.67, 0.87, and 0.78 nm, respectively. Moreover, the absorption spectra of the PCDTBT:PC_{71}BM active layers on different HTLs are consistent with each other (see Figure S3 in the Supporting Information), which indicates that the molecular

dx.doi.org/10.1021/am500336s | ACS Appl. Mater. Interfaces 2014, 6, 5122−5129

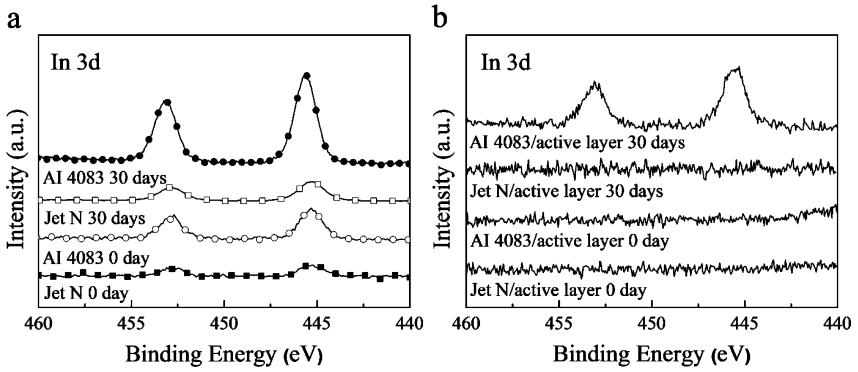

Figure 4. XPS spectra of indium in (a) different PEDOT:PSS layers, and (b) active layer (PCDTBT:$PC_{71}BM$) on different PEDOT:PSS layers after 0 days and 30 days storage in air.

orientation of the bulk active layer has not been affected by the different HTLs.

DEVICE STABILITY

The main goal of replacing the acidic PEDOT:PSS with the pH-neutral PEDOT:PSS is to improve the device lifetime. The stabilities of the devices were evaluated using a shelf-life method in which, after encapsulation, the devices were stored in a drybox in the dark under an ambient atmosphere at room temperature. The humidity inside the drybox was controlled at 50% RH during the entire experiment. Degradations of the active layer and of the top electrode by water and oxygen that permeated through the encapsulation clearly contribute to the overall stability of the device.[44,45] However, those factors are expected to be similar in all the devices and are beyond the scope of this study.

The normalized lifetime data are shown in Figure 3. The double-surface-treated Jet N device degrades much more slowly than the AI 4083 device. The PCE of the acidic PEDOT:PSS device decreases to 80% after 7 days, whereas the PCE of the pH-neutral PEDOT:PSS device decreases to 91%. After 50 days, the PCE of the acidic PEDOT:PSS device drops by 45%, whereas the PCE of the pH-neutral PEDOT:PSS device drops only by 20%. The improvement in the lifetime of the pH-neutral PEDOT:PSS is more than double. As illustrated in Figure 3, the trend in decreasing J_{SC} is the same as the trend in the PCE, which indicates that the reduction in the hole extraction efficiency at the interface of the HTL and the active layer substantially contributes to the loss of device performance. After 50 days, the J_{SC} of the acidic PEDOT:PSS device decreases by 34%, whereas the J_{SC} of the pH-neutral PEDOT:PSS device decreases only by 10%. In comparison, the V_{OC} of the acidic PEDOT:PSS device decreases by less than 10%, whereas the V_{OC} of the pH-neutral PEDOT:PSS device remains almost constant. Although the degradation is partly due to the chemical and morphological instability of the active layer and the corrosion of the metal cathode, the difference in the rate of degradation between the two devices is obvious.[25] Because the only difference between the devices is the HTL, we suspect that the acidic AI 4083 etches the ITO and causes the diffusion of indium into the HTL and the active layer, which destabilizes the device.

To verify this assumption, we conducted X-ray photoelectron spectroscopy (XPS) measurements on ITO/PEDOT:PSS samples and ITO/PEDOT:PSS/PCDTBT:$PC_{71}BM$ samples to detect the atomic concentration of indium. The XPS spectra are shown in Figure 4. On the bare ITO substrate, the atomic concentration of indium reaches 29.8%. As listed in Table 2, in the freshly prepared samples, 0.49% In is observed in the ITO/AI 4083 device, 0.08% In is detected in the ITO/double-treated Jet N device, and no trace of In is found in either the ITO/AI 4083/PCDTBT:$PC_{71}BM$ device or the ITO/doubled-treated Jet N/PCDTBT:$PC_{71}BM$ device. The data clearly show that the diffusion of In into the HTL most likely starts during the spin-coating process of PEDOT:PSS. By replacing the acidic PEDOT:PSS with neutral PEDOT:PSS, the ITO etching effect is dramatically reduced. After 15 days of storage under ambient conditions, the In content in the AI 4083 increases to 0.87%, and the In content in the Jet N increases to 0.40%. However, there is still no In detected in the active layer on either PEDOT:PSS sample. After 30 days of storage, the atomic concentration of indium further increases to 1.91% and 1.20% in the acidic PEDOT:PSS and pH-neutral PEDOT:PSS, respectively. Accordingly, the XPS spectra of In 3d that are shown in Figure 4a exhibit a more distinct peak profile in the AI 4083 sample than in the Jet N sample. In addition, 0.28% indium is found in the active layer that is above the acidic PEDOT:PSS, which suggests that the indium diffuses not only into the HTL but also into the photoactive layer. In contrast, no indium is detected in the active layer that is above the pH-neutral PEDOT:PSS, which shows that the rate of indium diffusion in the pH-neutral PEDOT:PSS is much lower than that in the acidic PEDOT:PSS. The diffused indium introduces gap states at the interface of the HTL and the active layer and inside the active layer. The gap states function as trapping sites of the photo-excited carriers, which leads to charge recombination and the reduction of the extracted photocurrent.[23,46,47] The faster diffusion of In that is observed in the acidic AI 4083 devices induces more gap states, thereby causing a more rapid degradation of the device.

Table 2. Atomic Concentration of Indium in Different PEDOT:PSS Layers and Active Layer on Different PEDOT:PSS Layers after 0 Days and 30 Days Storage in Air

	atomic concentration (%)			
	ITO/AI 4083	ITO/ Jet N	ITO/AI 4083/ active layer	ITO/Jet N/ active layer
fresh sample	0.49	0.08	0.00	0.00
15 days storage	0.87	0.40	0.00	0.00
30 days storage	1.91	1.20	0.28	0.00

CONCLUSIONS

The widely adopted HTL that is used in BHJ polymer solar cells, i.e., acidic PEDOT:PSS, is replaced with a pH-neutral PEDOT:PSS. UV-ozone and oxygen plasma treatments are used to reduce the energy level offset between the HTL and the active layer, which increases the open-circuit voltage, improves carrier transportation, and prevents carrier recombination. The performance of the devices with the pH-neutral PEDOT:PSS after the surface treatments is slightly better than that of the devices with the acidic PEDOT:PSS. The pH-neutral PEDOT:PSS reduces the etching of indium from the ITO substrate and slows down the penetration of indium into the active layer. As the result, the lifetime of the device is more than doubled. After 7 days of storage under ambient conditions, the PCE of the device with the acidic PEDOT:PSS decreases by 20%, whereas the PCE of the device with the pH-neutral PEDOT:PSS decreases by only 9%. After 50 days, the PCE of the device with the acidic PEDOT:PSS decreases by 45%, whereas the PCE of the device with the pH-neutral PEDOT:PSS decreases by 20%.

EXPERIMENTS AND METHODS

Materials. The ITO glasses were purchased from the China Southern Glass Holding Corp. The PEDOT:PSS (Clevios P VP AI 4083 and Clevios P Jet N) were purchased from H. C. Starck GmbH. PCDTBT and $PC_{71}BM$ were purchased from 1-material Chemscitech Inc. All the solvents used in the study were purchased from Aldrich. All chemicals and materials were purchased and used as received unless otherwise noted.

Device Fabrication. Patterned ITO glass substrates with a sheet resistance of 15 Ω/□ were cleaned sequentially in ultrasonic bath of acetone, isopropyl alcohol, detergent, deionized water, and isopropyl alcohol. After cleaning, the substrates were dried overnight in an oven at 80 °C. Prior to device fabrication, the substrates went through oxygen plasma for 20 min. Devices with six different HTLs were made: (A) AI 4083; (B) Jet N; (C) UV-ozone treated Jet N; (D) plasma-treated Jet N; (E) UV-ozone and plasma-treated Jet N; and (F) UV-ozone and plasma-treated AI 4083. The optimal HTLs' thicknesses are, respectively: (A) 40, (B) 20, (C) 10, (D) 10, (E) 10, and (F) 30 nm. Device A and B were prepared as follows: Clevios P VP AI 4083 and Clevios P Jet N were spin-coated on the substrates followed by 10 min annealing at 200 °C in nitrogen. For Device C, the Jet N film was exposed to UV-ozone in a UV-ozone oven for 5 min. For Device D, the Jet N film was treated with oxygen plasma for 5 min with a power of 80 W at 200 sccm oxygen flow. For Deivce E and F, the Jet N film and the AI 4083 film were treated with 5 min UV-ozone and 5 min oxygen plasma sequentially.

The solution of the active layer was made by mixing PCDTBT and $PC_{71}BM$ with a 1:4 weight ratio first, then dissolving the mixture in a blended solvent of 1,2-dichlorobenezene and chlorobenzene (3:1 by volume) and a concentration of 7 mg/mL. On top the PEDOT:PSS film, the active layer solution was spin-coated with a thickness of 80 nm. Solvent treatment on the active layer was carried out by spin-coating the a few drops of methanol. The aluminum electrode of 100 nm was deposited by thermal evaporation in a vacuum of about 3×10^{-4} Pa.

Device Characterizations and Film Studies. *J*−*V* characteristics of the devices were measured using a Keithley 2400 Source Measure Unit and an Air Mass 1.5 Global (AM 1.5 G) solar simulator (SAN-EI corporation, XES-40S1 150 W, AAA class, Japan) with irradiation intensity of 100 mW cm^{-2}. A shadow mask was attached to the device to define the light exposure area of 15.0 mm^2. EQE measurements were conducted using a monochromator (Newport 74125 monochromator equipped with 66984 ARC lamp). The incident light intensity was calibrated with a silicon photodiode.

The surface potentials and the work functions of the PEDOT:PSS films were obtained by Scanning Kelvin Probe Microscopy (Kelvin Probe 5050 Technology) in nitrogen. Each data point is the average value of 20 measurements on each sample. AFM images were obtained by a NanoScope NS3A system (Digital Instruments). Top view XPS analysis to determine the indium concentration at the samples' surfaces were performed on a Kratos Analytical Axis Ultra DLD X-ray Photoelectron Spectroscopy with a monochromated AlKα (1486.6 eV) X-ray source. All recorded peaks were corrected for electrostatic effects by setting the C−C component of the C_{1s} peak to 284.8 eV. The base pressure in the XPS analysis chamber was about 5×10^{-9} Torr. The probing depth of XPS is 5−8 nm.

ASSOCIATED CONTENT

Supporting Information

J−*V* characteristics of the OPV devices with different HTLs in dark, performance of the OPV devices with AI 4083 HTL and double treated Jet N HTL, AFM topographic images of the active layers on top of different HTLs, and the absorption spectra of the active layers on different HTLs are illustrated. This material is available free of charge via the Internet at http://pubs.acs.org.

AUTHOR INFORMATION

Corresponding Author

*E-mail: jianwang@scut.edu.cn.

Author Contributions

The manuscript was written through contributions of all authors. All authors have given approval to the final version of the manuscript.

Notes

The authors declare no competing financial interest.

ACKNOWLEDGMENTS

The authors are deeply grateful to the Ministry of Science and Technology (973 Program 2009CB623604, and 2009CB930604), and National Nature Science Foundation of China (61079116, 51373057) for their financial supports.

REFERENCES

(1) Yu, G.; Gao, J.; Hummelen, J. C.; Wudl, F.; Heeger, A. J. Polymer Photovoltaic Cells: Enhanced Efficiencies via a Network of Internal Donor-Acceptor Heterojunctions. *Science* **1995**, *270*, 1789−1791.

(2) Blom, P. W. M.; Mihailetchi, V. D.; Koster, L. J. A.; Markov, D. E. Device Physics of Polymer:Fullerene Bulk Heterojunction Solar Cells. *Adv. Mater.* **2007**, *19*, 1551−1566.

(3) Dennler, G.; Scharber, M. C.; Brabec, C. J. Polymer-Fullerene Bulk-Heterojunction Solar Cells. *Adv. Mater.* **2009**, *21*, 1323−1338.

(4) Chen, J. W.; Cao, Y. Development of Novel Conjugated Donor Polymers for High-Efficiency Bulk-Heterojunction Photovoltaic Devices. *Acc. Chem. Res.* **2009**, *42*, 1709−1718.

(5) Wang, W.; Wu, H.; Yang, C.; Luo, C.; Zhang, Y.; Chen, J.; Cao, Y. High-Efficiency Polymer Photovoltaic Devices from Regioregular Poly(3-hexylthiophene-2,5-diyl) and [6,6]-phenyl-C61-butyric Acid Methyl Ester Processed with Oleic Acid Surfactant. *Appl. Phys. Lett.* **2007**, *90*, 183512-1−183512-3.

(6) Ma, W. L.; Yang, C. Y.; Gong, X.; Lee, K.; Heeger, A. J. Thermally Stable, Efficient Polymer Solar Cells with Nanoscale Control of the Interpenetrating Network Morphology. *Adv. Funct. Mater.* **2005**, *15*, 1617−1622.

(7) Li, G.; Shrotriya, V.; Huang, J.; Yao, Y.; Moriarty, T.; Emery, K.; Yang, Y. High-Efficiency Solution Processable Polymer Photovoltaic Cells by Self-Organization of Polymer Blends. *Nat. Mater.* **2005**, *4*, 864−868.

(8) Seo, J. H.; Gutacker, A.; Sun, Y.; Wu, H.; Huang, F.; Cao, Y.; Scherf, U.; Heeger, A. J.; Bazan, G. C. Improved High-Efficiency Organic Solar Cells via Incorporation of a Conjugated Polyelectrolyte Interlayer. *J. Am. Chem. Soc.* **2011**, *133*, 8416−8419.

(9) Chen, L. M.; Hong, Z.; Li, G.; Yang, Y. Recent Progress in Polymer Solar Cells: Manipulation of Polymer:Fullerene Morphology and the Formation of Efficient Inverted Polymer Solar Cells. *Adv. Mater.* **2009**, *21*, 1434−1449.
(10) Kyaw, A. K.; Wang, D. H.; Wynands, D.; Zhang, J.; Nguyen, T. Q.; Bazan, G. C.; Heeger, A. J. Improved Light Harvesting and Improved Efficiency by Insertion of an Optical Spacer (ZnO) in Solution-Processed Small-Molecule Solar Cells. *Nano Lett.* **2013**, *13*, 3796−3801.
(11) He, Z.; Zhong, C.; Su, S.; Xu, M.; Wu, H.; Cao, Y. Enhanced Power-Conversion Efficiency in Polymer Solar Cells Using an Inverted Device Structure. *Nat. Photonics* **2012**, *6*, 593−597.
(12) Yang, T.; Wang, M.; Duan, C.; Hu, X.; Huang, L.; Peng, J.; Huang, F.; Gong, X. Inverted Polymer Solar Cells with 8.4% Efficiency by Conjugated Polyelectrolyte. *Energy Environ. Sci.* **2012**, *5*, 8208−8214.
(13) Lu, L.; Luo, Z.; Xu, T.; Yu, L. Cooperative Plasmonic Effect of Ag and Au Nanoparticles on Enhancing Performance of Polymer Solar Cells. *Nano Lett.* **2013**, *13*, 59−64.
(14) Li, X.; Choy, W. C.; Huo, L.; Xie, F.; Sha, W. E.; Ding, B.; Guo, X.; Li, Y.; Hou, J.; You, J.; Yang, Y. Dual Plasmonic Nanostructures for High Performance Inverted Organic Solar Cells. *Adv. Mater.* **2012**, *24*, 3046−3052.
(15) Yoo, J. E.; Lee, K. S.; Garcia, A.; Tarver, J.; Gomez, E. D.; Baldwin, K.; Sun, Y.; Meng, H.; Nguyen, T. Q.; Loo, Y. L. Directly Patternable, Highly Conducting Polymers for Broad Applications in Organic Electronics. *Proc. Natl. Acad. Sci. U.S.A.* **2010**, *107*, 5712−5717.
(16) Betancur, R.; Maymó, M.; Elias, X.; Vuong, L. T.; Martorell, J. Sputtered NiO as Electron Blocking Layer in P3HT:PCBM Solar Cells Fabricated in Ambient Air. *Sol. Energy Mater. Sol. Cells* **2011**, *95*, 735−739.
(17) Sun, Y.; Takacs, C. J.; Cowan, S. R.; Seo, J. H.; Gong, X.; Roy, A.; Heeger, A. J. Efficient, Air-Stable Bulk Heterojunction Polymer Solar Cells Using MoO_x as the Anode Interfacial Layer. *Adv. Mater.* **2011**, *23*, 2226−2230.
(18) Shrotriya, V.; Li, G.; Yao, Y.; Chu, C. W.; Yang, Y. Transition Metal Oxides as the Buffer Layer for Polymer Photovoltaic Cells. *Appl. Phys. Lett.* **2006**, *88*, 073508−1-073508-3.
(19) Han, S.; Shin, W. S.; Seo, M.; Gupta, D.; Moon, S. J.; Yoo, S. Improving Performance of Organic Solar Cells Using Amorphous Tungsten Oxides as an Interfacial Buffer Layer on Transparent Anodes. *Org. Electron.* **2009**, *10*, 791−797.
(20) Garcia, A.; Welch, G. C.; Ratcliff, E. L.; Ginley, D. S.; Bazan, G. C.; Olson, D. C. Improvement of Interfacial Contacts for New Small-Molecule Bulk-Heterojunction Organic Photovoltaics. *Adv. Mater.* **2012**, *24*, 5368−5373.
(21) Murase, S.; Yang, Y. Solution Processed MoO_3 Interfacial Layer for Organic Photovoltaics Prepared by a Facile Synthesis Method. *Adv. Mater.* **2012**, *24*, 2459−2462.
(22) Teran-Escobar, G.; Pampel, J.; Caicedo, J. M.; Lira-Cantu, M. Low-Temperature, Solution-Processed, Layered V_2O_5 Hydrate as the Hole-Transport Layer for Stable Organic Solar Cells. *Energy Environ. Sci.* **2013**, *6*, 3088−3098.
(23) Schlatmann, A. R.; Floet, D. W.; Hilberer, A.; Garten, F.; Smulders, P. J. M.; Klapwijk, T. M.; Hadziioannou, G. Indium Contamination from the Indium-Tin-Oxide Electrode in Polymer Light-Emitting Diodes. *Appl. Phys. Lett.* **1996**, *69*, 1764−1766.
(24) de Jong, M. P.; van Ijzendoorn, L. J.; de Voigt, M. J. A. Stability of the Interface between Indium-Tin-Oxide and Poly(3,4-ethylenedioxythiophene)/Poly(styrenesulfonate) in Polymer Light-Emitting Diodes. *Appl. Phys. Lett.* **2000**, *77*, 2255−2257.
(25) Jorgensen, M.; Norrman, K.; Gevorgyan, S. A.; Tromholt, T.; Andreasen, B.; Krebs, F. C. Stability of Polymer Solar Cells. *Adv. Mater.* **2012**, *24*, 580−612.
(26) Wong, K. W.; Yip, H. L.; Luo, Y.; Wong, K. Y.; Lau, W. M.; Low, K. H.; Chow, H. F.; Gao, Z. Q.; Yeung, W. L.; Chang, C. C. Blocking Reactions between Indium-Tin Oxide and Poly (3,4-ethylene dioxythiophene):Poly(styrene sulphonate) with a Self-Assembly Monolayer. *Appl. Phys. Lett.* **2002**, *80*, 2788−2790.
(27) Kim, H.; Nam, S.; Lee, H.; Woo, S.; Ha, C. S.; Ree, M.; Kim, Y. Influence of Controlled Acidity of Hole-Collecting Buffer Layers on the Performance and Lifetime of Polymer:Fullerene Solar Cells. *J. Phys. Chem. C* **2011**, *115*, 13502−13510.
(28) Wu, S.; Han, S.; Zheng, Y.; Zheng, H.; Liu, N.; Wang, L.; Cao, Y.; Wang, J. Ph-Neutral PEDOT:PSS as Hole Injection Layer in Polymer Light Emitting Diodes. *Org. Electron.* **2011**, *12*, 504−508.
(29) Wang, Q.; Zhou, Y.; Zheng, H.; Shi, J.; Li, C.; Su, C. Q.; Wang, L.; Luo, C.; Hu, D.; Pei, J.; Wang, J.; Peng, J.; Cao, Y. Modifying Organic/Metal Interface via Solvent Treatment to Improve Electron Injection in Organic Light Emitting Diodes. *Org. Electron.* **2011**, *12*, 1858−1863.
(30) Zhou, H.; Zhang, Y.; Seifter, J.; Collins, S. D.; Luo, C.; Bazan, G. C.; Nguyen, T. Q.; Heeger, A. J. High-Efficiency Polymer Solar Cells Enhanced by Solvent Treatment. *Adv. Mater.* **2013**, *25*, 1646−1652.
(31) Liu, X.; Wen, W.; Bazan, G. C. Post-Deposition Treatment of an Arylated-Carbazole Conjugated Polymer for Solar Cell Fabrication. *Adv. Mater.* **2012**, *24*, 4505−4510.
(32) Ye, L.; Jing, Y.; Guo, X.; Sun, H.; Zhang, S.; Zhang, M.; Huo, L.; Hou, J. Remove the Residual Additives toward Enhanced Efficiency with Higher Reproducibility in Polymer Solar Cells. *J. Phys. Chem. C* **2013**, *117*, 14920−14928.
(33) Moon, J. M.; Bae, J. H.; Jeong, J. A.; Jeong, S. W.; Park, N. J.; Kim, H. K.; Kang, J. W.; Kim, J. J.; Yi, M. S. Enhancement of Hole Injection Using Ozone Treated Ag Nanodots Dispersed on Indium Tin Oxide Anode for Organic Light Emitting Diodes. *Appl. Phys. Lett.* **2007**, *90*, 163516-1−163516-3.
(34) Milliron, D. J.; Hill, I. G.; Shen, C.; Kahn, A.; Schwartz, J. Surface Oxidation Activates Indium Tin Oxide for Hole Injection. *J. Appl. Phys.* **2000**, *87*, 572−576.
(35) Siebert-Henze, E.; Lyssenko, V. G.; Fischer, J.; Tietze, M.; Brueckner, R.; Menke, T.; Leo, K.; Riede, M. Electroabsorption Studies of Organic P-I-N Solar Cells: Increase of the Built-in Voltage by Higher Doping Concentration in the Hole Transport Layer. *Org. Electron.* **2014**, *15*, 563−568.
(36) Giebink, N. C.; Wiederrecht, G. P.; Wasielewski, M. R.; Forrest, S. R. Ideal Diode Equation for Organic Heterojunctions. I. Derivation and Application. *Phys. Rev. B* **2010**, *82*, 155305-1−155305-12.
(37) Heeger, A. J. 25th Anniversary Article: Bulk Heterojunction Solar Cells: Understanding the Mechanism of Operation. *Adv. Mater.* **2014**, *26*, 10−28.
(38) Yip, H. L.; Jen, A. K. Y. Recent Advances in Solution-Processed Interfacial Materials for Efficient and Stable Polymer Solar Cells. *Energy Environ. Sci.* **2012**, *5*, 5994−6011.
(39) Ratcliff, E. L.; Zacher, B.; Armstrong, N. R. Selective Interlayers and Contacts in Organic Photovoltaic Cells. *J. Phys. Chem.* **2011**, *2*, 1337−1350.
(40) Brabec, C. J.; Cravino, A.; Meissner, D.; Sariciftci, N. S.; Fromherz, T.; Rispens, M. T.; Sanchez, L.; Hummelen, J. C. Origin of the Open Circuit Voltage of Plastic Solar Cells. *Adv. Funct. Mater.* **2001**, *11*, 374−380.
(41) Mihailetchi, V. D.; Blom, P. W. M.; Hummelen, J. C.; Rispens, M. T. Cathode Dependence of the Open-Circuit Voltage of Polymer:Fullerene Bulk Heterojunction Solar Cells. *J. Appl. Phys.* **2003**, *94*, 6849−6854.
(42) Xu, Z.; Chen, L. M.; Yang, G.; Huang, C. H.; Hou, J.; Wu, Y.; Li, G.; Hsu, C. S.; Yang, Y. Vertical Phase Separation in Poly(3-hexylthiophene): Fullerene Derivative Blends and Its Advantage for Inverted Structure Solar Cells. *Adv. Funct. Mater.* **2009**, *19*, 1227−1234.
(43) Saracco, E.; Bouthinon, B.; Verilhac, J. M.; Celle, C.; Chevalier, N.; Mariolle, D.; Dhez, O.; Simonato, J. P. Work Function Tuning for High-Performance Solution-Processed Organic Photodetectors with Inverted Structure. *Adv. Mater.* **2013**, *25*, 6534−6538.
(44) Wang, M.; Xie, F.; Du, J.; Tang, Q.; Zheng, S.; Miao, Q.; Chen, J.; Zhao, N.; Xu, J. B. Degradation Mechanism of Organic Solar Cells

with Aluminum Cathode. *Sol. Energy Mater. Sol. Cells* **2011**, *95*, 3303−3310.
(45) Song, Q. L.; Wang, M. L.; Obbard, E. G.; Sun, X. Y.; Ding, X. M.; Hou, X. Y.; Li, C. M. Degradation of Small-Molecule Organic Solar Cells. *Appl. Phys. Lett.* **2006**, *89*, 251118-1−251118-3.
(46) Wu, B.; Wu, X.; Guan, C.; Fai Tai, K.; Yeow, E. K.; Jin Fan, H.; Mathews, N.; Sum, T. C. Uncovering Loss Mechanisms in Silver Nanoparticle-Blended Plasmonic Organic Solar Cells. *Nat. Commun.* **2013**, *4*, 2004-1−2004-7.
(47) Dou, L.; You, J.; Hong, Z.; Xu, Z.; Li, G.; Street, R. A.; Yang, Y. 25th Anniversary Article: A Decade of Organic/Polymeric Photovoltaic Research. *Adv. Mater.* **2013**, *25*, 6642−6671.